

Many-body effects on excitonic optical properties of photoexcited semiconductor quantum wire structures

D. W. Wang and S. Das Sarma

Department of Physics, University of Maryland, College Park, Maryland 20742-4111

(Received 26 February 2001; published 17 October 2001)

We study carrier-interaction-induced many-body effects on the excitonic optical properties of highly photoexcited one-dimensional semiconductor quantum wire systems by solving the dynamically screened Bethe-Salpeter equation using realistic Coulomb interaction between carriers. Including dynamical screening effects in the electron-hole self-energy and in the electron-hole interaction vertex function, we find that the excitonic absorption is essentially peaked at a constant energy for a large range of photoexcitation density ($n=0-6 \times 10^5 \text{ cm}^{-1}$), above which the absorption peak disappears without appreciable gain; i.e., no exciton to free electron-hole plasma Mott transition is observed, in contrast to previous theoretical results but in agreement with recent experimental findings. This absence of gain (or the nonexistence of a Mott transition) arises from the strong inelastic scattering by one-dimensional plasmons or charge density excitations, closely related to the non-Fermi-liquid nature of one-dimensional systems. Our theoretical work demonstrates a transition or a crossover in one-dimensional photoexcited electron-hole systems from an effective Fermi liquid behavior associated with a dilute gas of noninteracting excitons in the low-density region ($n < 10^5 \text{ cm}^{-1}$) to a non-Fermi liquid in the high-density region ($n > 10^5 \text{ cm}^{-1}$). The conventional quasistatic approximation for this problem is also carried out to compare with the full dynamical results. Numerical results for exciton binding energy and absorption spectra are given as functions of carrier density and temperature.

DOI: 10.1103/PhysRevB.64.195313

PACS number(s): 78.55.-m, 71.35.Cc, 78.66.Fd, 73.21.-b

I. INTRODUCTION

Excitons in low-dimensional semiconductor systems have been extensively studied in the recent past. Present interest has focused on one-dimensional excitons in artificially structured semiconductor quantum wire (QWR) systems where spectacular improvements in growth and nanofabrication techniques have led to very narrow wires of nanostructure size ($< 100 \text{ \AA}$ in GaAs) with rather deep conduction band electron confinement energy ($\sim 150 \text{ meV}$) and large conduction-subband spacing ($\sim 20 \text{ meV}$) (Refs. 1–4) so that the electrons in the conduction band of such a QWR most likely form a pure one-dimensional (1D) system. For the holes in the QWR valence band, the bare confinement potential (for example, in the GaAs-AlGaAs system) is known to be too shallow ($\sim 10 \text{ meV}$) for a hole to be one dimensionally confined in these QWR structures. Including the Coulomb interaction between electrons and holes along the transverse (i.e., perpendicular to the 1D free motion direction) directions of the wire, however, Glutsch *et al.*⁵ find that even the holes in the valence band of QWR's can be strongly localized in the transverse plane, leading to both electrons and holes being effectively 1D (or rather quasi-1D) in the dynamical sense. Therefore an exciton in such ultranarrow QWR nanostructures can be effectively thought of as a bound pair of a 1D electron and a 1D hole with the carrier dynamics being free along the 1D wire direction as long as one is interested in low energy (lower than confinement energy $\sim 20-100 \text{ meV}$) excitonic optical properties. Such strong confinement for both electrons and holes also substantially enhances the excitonic binding energy, leading to novel optical phenomena. In the low- (electron-hole) density limit without considering the self-energy correction to the conduc-

tion and the valence-band energies as well as neglecting all dynamical screening effects, the single-electron and single-hole problem in forming the exciton can be exactly solved as a quasi-1D hydrogenic (Wannier exciton) atom with an exciton radius of about 100 \AA for GaAs-based QWR systems. This single-1D-exciton problem, where an electron and a hole in a QWR form a bound excitonic state, has been studied extensively in the recent literature in the context of understanding QWR excitonic optical properties. Such a noninteracting exciton picture, based on a simple single-particle electron-hole hydrogenic bound-state scenario, obviously only applies in the dilute low-carrier-density limit when the excitons or the bound electron-hole pairs are effectively very far from each other, forming a noninteracting exciton gas. We will refer to this situation as a Fermi liquid (because in 1D only an effectively noninteracting system may behave as a Fermi liquid) or a noninteracting exciton gas. In the high-carrier-density situation the excitons must overlap with each other a great deal, and the simple Fermi liquid picture of a noninteracting exciton gas would not apply. Our main goal in this paper is to theoretically study this transition between the low-density (Fermi-liquid-like) exciton gas and the high density system of interacting (and strongly overlapping) excitons in quasi-1D semiconductor (GaAs) QWR systems. This exciton gas to a strongly overlapping and highly correlated electron-hole system crossover with increasing electron-hole density can be thought of as a transition from an insulating exciton gas to a conducting electron-hole plasma (EHP), the Mott transition. A typical feature of this Mott transition, observed in higher-dimensional (2D,3D) optical experiments, is the development of optical gain in the absorption spectra where the absorption coefficient becomes negative (gain region) in some frequency range. One of the questions addressed in this paper is whether such an optical gain region

exists in 1D photoexcited QWR systems. In this paper we consider the formation, stability, and optical properties of one-dimensional excitons from low to high carrier densities in semiconductor QWR's under photoexcitation conditions (i.e., equal electron and hole densities), a problem which has attracted a great deal of both theoretical⁵⁻¹⁸ and experimental¹⁻⁴ attention in these years. Consistent with recent interest one of the central issues we focus on is the density-induced exciton gas to EHP Mott transition in 1D QWR systems and its experimental signature.

The motivation of our work arises from recent experimental studies of the photoluminescence spectra of 1D GaAs/Al_{1-x}Ga_xAs semiconductor QWR systems.¹⁻⁴ The experimentalists use strong lasers to pump photons into the QWR systems, exciting electrons from the filled valence band into the empty conduction band and/or the exciton levels, and observe the spectrum of the subsequently emitted light coming from the eventual recombination of the excited electrons and the holes created in the valence band. The photoluminescence spectrum is proportional to the exciton-EHP optical oscillator strength, which, at first sight (i.e., without incorporating the Sommerfeld factor effect associated with the electron-hole Coulomb interaction), is expected to have an $\omega^{-1/2}$ singularity at the band-gap energy due to the $E^{-1/2}$ divergence of the 1D electron density of states¹⁸ at band edge. However, this 1D plasma band-edge singularity is known to be strongly suppressed by the excitonic Coulomb correlation effect¹⁰ so that the main peak observed in the experimental photoluminescence spectra should result from the excitonic effect rather than the band-edge singularity of the noninteracting electron-hole plasma. The most striking experimental observation in the recent¹⁻⁴ experimental studies of photoexcited QWR systems has been the finding^{1,2} that the exciton peak seems to be at an almost constant energy independent of the carrier density, i.e., independent of the laser pumping power. Thus the exciton peak seems to remain well defined (and unshifted in energy) all the way from very low to very high photoexcitation density ($\sim 3 \times 10^6 \text{ cm}^{-11}$) without any distinct signature of the expected insulator-(exciton-) to-metal (EHP) Mott transition and the associated optical gain. The constancy of the exciton energy could, in principle, arise from an almost exact cancellation between the exchange-correlation induced shrinking of the nominal band gap, the so-called band gap renormalization (BGR), and the reduction of the exciton binding energy (with respect to the bottom of the renormalized band edge) due to the screening induced softening of the Coulomb interaction.⁶ Such an accidental cancellation between two distinct physical mechanisms (namely, BGR and screening suppression of exciton energy) over a wide range of photoexcitation density needs to be theoretically established in a compelling way.⁶ In addition, combining this accidental cancellation explanation with the experimental fact of a very high Mott density (not yet seen experimentally) one may conclude that the BGR of a 1D electron-hole ($e-h$) system should be very weak in the high-density situation, which is not consistent with theoretical calculations up to now.^{4,15,16} In particular, one must understand why there is no characteristic signature of the EHP in the luminescence spectra even at very high photoexcita-

tion densities. One must be able to answer the question as to where the Mott transition has gone. On this issue, an important and unresolved problem for the photoluminescence experiment is that there is no reliable and direct way of estimating the photoexcited electron-hole density in such highly pumped QWR systems. The theoretical basis of the density estimation methods in the literature,¹ such as from the line shape analysis of the spectrum, is usually not self-consistent and not appropriate in such high-density strongly laser-pumped systems. Although we feel that the precise carrier density of the photoexcited QWR systems may not be known accurately, this issue does not pose any fundamental problem for our theory where the EHP density $n = n_e = n_h$ is an input parameter. The problem arises only in trying a direct quantitative comparison with experiments.¹⁻³

From the theoretical point of view, the full many-body calculation in a high-electron-hole-density semiconductor system is complicated and has not been attempted before except for our own short Letter published last year.⁶ The exciton mode is a solution of the Bethe-Salpeter equation (BSE) for the interaction vertex which, in the many-particle situation of interest to us, should include self-energy and dynamical screening correlations. A complete or exact solution of the BSE is only possible in the dilute exciton limit when it reduces to a simple hydrogenic electron-hole bound-state Schrödinger equation. Our interest in this paper is in the many-particle "exciton" state in the photoexcited semiconductor QWR system where self-energy correlations of simple electron or hole states and dynamical screening of the electron-hole Coulomb interaction vertex are important. A model of an electron gas with a single hole in a wire¹⁷ is not appropriate in our problem because a bound state always exists in any attractive potential in 1D systems, which will trivially provide an overestimate of the Mott density. We emphasize that both the quasiparticle self-energy and the dynamical screening of the electron-hole interaction vertex should be included properly (i.e., consistent with each other in a conserving approximation) in the BSE to obtain the correct description of the Mott transition. With the exception of our own short earlier report⁶ most other theoretical calculations use the static (Hartree-Fock) approximation or the quasistatic approximation¹⁸ to the self-energy and a statically screened interaction vertex to solve the many-particle BSE and obtain the optical absorption-gain spectra. In these simpler approximations, where dynamical screening effects are neglected in an uncontrolled way, the dominant excitonic peak has a weak redshift (a few meV decrease) with increasing density up to a Mott density n_c , above which the excitonic peak completely disappears and the spectrum shows a shallow (and weak) gain region very similar to the behavior of the noninteracting EHP.^{7,10,14,17} Including the many-body dynamical screening⁶ in the Coulomb interaction, the exciton peak stays essentially constant in energy (for $n < n_c$) and exhibits a pronounced gain spectrum (for $n > n_c$), stronger than the quasistatic results. But the predicted Mott densities in the above theories ($n_c \sim 8 \times 10^4 - 8 \times 10^5 \text{ cm}^{-1}$) are all below the experimentally estimated value ($n_c > 3 \times 10^6 \text{ cm}^{-1}$) — in fact, it is not clear if experimentally the transition to the EHP has ever been observed even at the

highest photoexcitation densities. It is in general hard to include the many-body effects appropriately in a calculationally tractable model over such a wide range of density (over at least four orders of magnitude in n), from the weak-coupling dilute exciton gas system to the strong-coupling EHP regime.

In this paper, starting with the realistic Coulomb interaction in 1D T-shaped QWR systems, we first evaluate the single-particle self-energy for both electrons and holes in the dynamical plasmon pole approximation (PPA) within the so-called GW scheme (i.e., in the leading-order dynamically screened interaction) to obtain the electron and hole renormalized Green's function. This self-energy calculation, which by itself does not contain any direct excitonic effects, gives us the BGR or the reduction of the nominal band gap due to exchange correlation. For comparison, we also calculate the BGR obtained by the quasistatic calculation in both static random phase approximation (RPA) and static PPA in this paper. We then derive analytically the effective electron-hole (e - h) interaction vertex $V_{eff}(k, \omega)$, which includes consistently the electron-hole-plasmon coupling with the external photons within our dynamical GW-RPA-PPA approximation scheme. We use two different methods to study the excitonic properties: one is a variational approximation on an effective exciton Hamiltonian,¹⁸ which depends on the carrier density; the other technique is to solve the dynamical BSE by treating both self-energy renormalization and vertex correction (arising from the Coulomb interaction) on an equal footing (within our plasmon pole approximation scheme), obtaining the optical absorption spectra. Both calculations are carried out over a wide range of e - h density from $n = 10^2 \text{ cm}^{-1}$ to $n = 10^6 \text{ cm}^{-1}$ at finite temperatures under the quasiequilibrium condition; i.e., the e - h density is assumed to be a constant parameter for each density calculation (and $n = n_e = n_h$). While our dynamical BSE calculation includes exciton and EHP effects equivalently and is directly capable of providing the Mott density n_c through the analysis of the absorption spectra, the variational exciton energy has to be compared with the BGR calculation in order to ascertain the Mott transition — in particular, the merging of the effective variational exciton with the renormalized band edge is taken to be the signal for a Mott transition. We find that the absorption peak obtained from solving the dynamical BSE survives with very large broadening well above the critical density n_c estimated from the variational approximation, and no optical gain (negative absorption) regime shows up in the spectra even at the highest e - h density. This implies the *nonexistence* of Mott transition in 1D electron-hole systems. This striking result may be physically understood as arising from the fact that the quasiparticle picture underlying the conventional Fermi liquid model fails in high-density 1D systems due to strong inelastic scattering by plasmons, associated with the generic non-Fermi-liquid behavior in 1D systems. In fact, in 1D systems there is no conventional EHP because there are no single-particle excitations in an interacting 1D systems. This nonexistence of single-particle excitations or quasiparticles also leads to a breakdown of the conventional exciton picture — a quasielectron and a quasihole bound pair. We will discuss this point in

more details later in this paper.

This paper is organized as follows: In Sec. II we present and discuss the theory we use in various parts of our calculations, e.g., the realistic Coulomb interaction in the 1D T-shaped QWR system, the single-particle self-energy calculation in the single-loop PPA-GW approximation, the different approximation schemes used for screening the long-ranged Coulomb interaction, the dynamical Bethe-Salpeter equation approximations in our theory, and the effective exciton Hamiltonian used in the variational calculation. In Sec. III we show our results for the density-dependent exciton energy in the variational method and for the excitonic optical properties from the solution of BSE. In Sec. IV we conclude with a discussion and a summary of our results.

II. THEORY

We use the two-band (one-conduction-band and one-valence-band) model to study the 1D electron-hole system, neglecting higher subbands and the degenerate valence bands. We also consider the photoexcited quasiequilibrium regime where the e - h density is assumed to be a constant (in time) so that the Hamiltonian of such a 1D electron-hole system can be expressed as (in the effective mass approximation and assuming purely parabolic band dispersion; we take $\hbar = 1$ throughout)

$$\begin{aligned}
 H = & \sum_k \left(E_g^0 + \frac{k^2}{2m_e} c_k^\dagger c_k + \frac{k^2}{2m_h} d_k^\dagger d_k \right) \\
 & + \frac{1}{2L} \sum_{k, k', q} [V_{c,ee}(q) c_{k-q}^\dagger c_{k'+q}^\dagger c_{k'} c_k + V_{c,hh}(q) \\
 & \times d_{k-q}^\dagger d_{k'+q}^\dagger d_{k'} d_k - 2V_{c,eh}(q) c_{k-q}^\dagger c_k d_{k'+q}^\dagger d_{k'}], \tag{1}
 \end{aligned}$$

where c_k (c_k^\dagger) and d_k (d_k^\dagger) are the annihilation (creation) operators for conduction-band electrons and valence-band holes, respectively (we will not explicitly show the spin index in summations throughout this paper although spin is included in our calculations), and $m_{e/h}$ are the electron-hole effective masses. E_g^0 is the direct band gap between the top of the valence band and the bottom of the conduction band, taken to be 1550 meV for the GaAs/Al_{1-x}Ga_xAs QWR system in all our calculations. There are three different Coulomb interactions entering the Hamiltonian: electron-electron [$V_{c,ee}(q)$], hole-hole [$V_{c,hh}(q)$], and electron-hole [$V_{c,eh}(q)$] interactions. The first two give rise to the electron and hole quasiparticle self-energies and the other one, the electron-hole interaction, produces the exciton bound state. One should note that if we neglect the self-energy correction and also dynamical screening effect (i.e., the low-density limit of a Wannier exciton), the Hamiltonian of Eq. (1) leads to a 1D hydrogen atom problem¹⁹ for the Wannier exciton, which in 1D always has a bound excitonic state even for an arbitrarily weak electron-hole (attractive) interaction. Using a model of an electron gas with a single hole therefore gives rises a very high Mott density estimate (even if $V_{c,eh}$ is statically screened), which is a reflection of this 1D bound-state

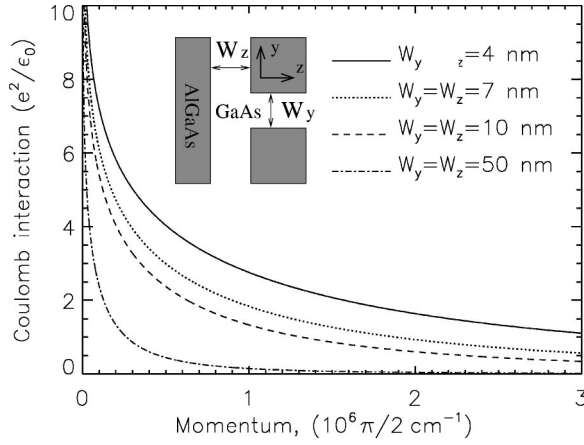


FIG. 1. Theoretically calculated [from Eqs. (2)–(4)] 1D Coulomb interaction in a T-shaped QWR system in momentum space. Results of different wire widths are calculated and shown together. In the inset we show the T-shaped intersection of two quantum wells in cross section.

property. We address both the many-body self-energy effect and the electron-hole excitonic binding effect on an equal footing in the theory, which we accomplish by using the dynamical Bethe-Salpeter equation as described below.

A. Coulomb interaction in QWR's

The realistic (bare) Coulomb interaction in 1D QWR's is obtained by taking the expectation value of the 3D Coulomb interaction over the electron wave function along the transverse directions (y and z axes; see the inset of Fig. 1) of the wire. After Fourier transformation along the 1D wire direction (x), we have^{12,15,20} for the Coulomb interaction matrix element

$$\begin{aligned}
 V_{c,ij}(q) &= \frac{e^2}{\epsilon_0} \int_{-\infty}^{\infty} dy dy' \int_{-\infty}^{\infty} dz dz' \int_{-\infty}^{\infty} dx \\
 &\quad \times \frac{e^{-iqx} |\phi_i(y,z)|^2 |\phi_j(y',z')|^2}{\sqrt{x^2 + (y-y')^2 + (z-z')^2}} \\
 &= \frac{2e^2}{\epsilon_0} \int_{-\infty}^{\infty} dy dy' \int_{-\infty}^{\infty} dz dz' |\phi_i(y,z)|^2 \\
 &\quad \times |\phi_j(y',z')|^2 K_0[q \sqrt{(y-y')^2 + (z-z')^2}],
 \end{aligned} \tag{2}$$

where $\phi_i(y,z)$ is the QWR confinement wave function for the lowest eigenstate of electrons ($i=e$) or holes ($i=h$). Their exact forms depend on the geometry and the detailed nature of confinement for the QWR system. $K_0(x)$ is the zeroth-order modified Bessel function of the second kind²⁰ which diverges logarithmically when x goes to zero (i.e., in the long-wavelength limit).

Following the experimental system of Ref. 2, we use T-shaped QWR parameters to numerically calculate the 1D Coulomb interaction via Eq. (2). To simplify calculations (and also to have some analytical control) we use the follow-

ing two approximations in evaluating the wave function $\phi_i(y,z)$: (i) we assume the confinement potential for both electrons and holes to be infinitely deep—i.e., both electrons and holes are completely confined by the 2D T-shaped potential well—so that the wave functions of electrons and holes are of the same form, independent of their effective mass difference. Consequently the three different interactions ($V_{c,ee}$, $V_{c,hh}$, and $V_{c,eh}$) become the same, denoted by V_c throughout this paper. This simplifying approximation is justified by the detailed work of Ref. 5, as mentioned in the Introduction. (ii) Instead of numerically solving the complicated 2D Schrödinger equation to get the ground-state single-particle wave function^{5,12,13} (which is not the focus of our interest), we simply approximate $\phi(y,z)$ to be the product of two single-variable functions $\xi(y)$ and $\psi(z)$ [i.e., $\phi(y,z) \sim \xi(y)\psi(z)$] and assume²¹ a simple and reasonable approximate model form for $\xi(y)$ and $\psi(z)$ through the following exponential formulas:

$$\xi(y) = \frac{2^{3/4}}{W_y^{1/2} \pi^{1/4}} e^{-(2y/W_y)^2}, \tag{3}$$

$$\psi(z) = \frac{2^{5/2} z}{W_z^{3/2}} e^{-2z/W_z}, \tag{4}$$

where W_z and W_y are the full-plane (x - y plane) QW width and the half-plane (x - z plane) QW width, respectively. Equations (3) and (4) have the maximum electron-hole density at $y=0$, $z=W_z/2$, with three branches of exponentially decaying density along $\pm y$ and $+z$ directions (see the inset of Fig. 1). The exponential decaying lengths or confinement sizes are $W_y/2$ and $W_z/2$ in y and z directions, respectively, and thus in our model of the T-shaped QWR the effect of wire geometry on the Coulomb interaction is entirely contained in the effective “wire sizes” W_y and W_z , which are the confinement parameters of our model. This approximation greatly simplifies the calculation of the realistic Coulomb interaction in Eq. (2) and makes our BSE calculations tractable. We believe our QWR confinement model, as defined in Eqs. (3) and (4), to be quite reasonable.²¹ For example, the exciton binding energy calculated in this approximation is 18.2 meV for $W_y=W_z=7$ nm wire, very close to the quoted experimental value, 17 meV, for the same wire size.² The small overestimate (about 7%) is expected because of the assumption of infinite confinement energy and the strong e^{-y^2} localization of $\xi(y)$. In more accurate numerical treatments the confinement is weaker than in our model, leading to a lower binding energy in the QWR system. In Fig. 1 we show the calculated $V_c(q)$ from Eqs. (2)–(4) for different wire sizes. We assume only one (the ground) electron and hole subband in the conduction and valence band, respectively.

B. Absorption spectra

In order to study the excitonic effect on optical properties of 1D photoexcited electron-hole systems in semiconductor QWR structures, we calculate the dynamical (photon-

frequency-dependent) absorption coefficient $\alpha(\omega)$ and refractive index $n(\omega)$, which are related to the long-wavelength dielectric function $\varepsilon(q \rightarrow 0, \omega)$, by the following formula:

$$n(\omega) + i \frac{c\alpha(\omega)}{2\omega} = \varepsilon(\omega)^{1/2}, \quad (5)$$

where c is the vacuum light velocity. The dynamical refractive index $n(\omega)$ is therefore given in terms of $\varepsilon(\omega)$ by

$$n(\omega) = \sqrt{\frac{1}{2} \{ \text{Re } \varepsilon(\omega) + [\text{Re } \varepsilon(\omega)^2 + \text{Im } \varepsilon(\omega)^2]^{1/2} \}}, \quad (6)$$

and the absorption coefficient $\alpha(\omega)$ is given by

$$\alpha(\omega) = \frac{\omega \text{Im } \varepsilon(\omega)}{n(\omega)c}. \quad (7)$$

Using the linear response theory,^{18,22} the dielectric function of the 1D e - h system is expressed as

$$\varepsilon(\omega) \simeq \varepsilon_\infty - \frac{4\pi e^2}{AL} \sum_{k,k'} r_{vc}(k) r_{vc}^*(k') G_{q \rightarrow 0}(k, k', \omega), \quad (8)$$

where the retarded pair Green's function $G_q(k, k', \omega)$ is

$$G_q(k, k', \omega) = -i \int_0^\infty e^{i\omega t} \langle [d_{-k}(t) c_{k+q}(t), c_{k'+q}^\dagger(0) d_{-k'}^\dagger(0)]_0 \rangle dt, \quad (9)$$

and $A = W_y W_z$ is the cross-sectional area of the QWR. In these equations q is the center of mass momentum of the exciton which is set to zero (and hence not shown explicitly) in all our calculations below. $r_{vc}(k)$ is the dipole matrix element, which can be simplified in the effective mass approximation:¹⁸

$$|r_{vc}(k)| \simeq \frac{M(k)}{\sqrt{4mE_g^0}}, \quad (10)$$

where the reduced mass $m = m_e m_h / (m_e + m_h)$ and

$$M(k) = \left(1 + \frac{k^2}{2mE_g^0} \right)^{-1}. \quad (11)$$

By introducing a new function

$$Q(k, \omega) = \sum_{k'} M(k') G(k, k', \omega), \quad (12)$$

the dielectric function in Eq. (8) can be expressed as

$$\varepsilon(\omega) \simeq \varepsilon_\infty - \frac{\pi e^2}{ALmE_g^0} \sum_k M(k) Q(k, \omega), \quad (13)$$

and the dynamical function $Q(k, \omega)$, which is essentially a two-particle Green's function, satisfies the Bethe-Salpeter equation described below.

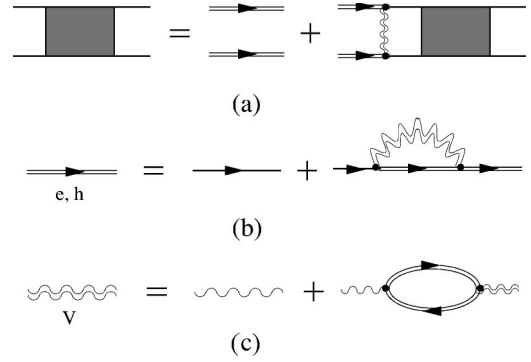


FIG. 2. Many-body Feynman diagrams used in the paper with the single (double) solid line representing the bare (dressed) electron or hole Green's function and the single (double) wavy line representing the bare (dressed) Coulomb interaction: (a) the excitonic Bethe-Salpeter equation, (b) the single-loop self-energy (in the so-called GW approximation) defining the dressed Green's function, and (c) the RPA dressing of the Coulomb interaction (treated in the plasmon-pole approximation in our calculation).

C. Bethe-Salpeter equations

For the results to be presented in this paper, the many-body exciton is given by the so-called Bethe-Salpeter equation¹⁸ for the two-particle Green's function shown diagrammatically in Fig. 2(a), which corresponds to a rather complex set of two-component (electrons and holes) coupled nonlinear integral equations which must be solved self-consistently with the bare interaction being the Coulomb interaction in the QWR geometry. These equations are notoriously difficult to solve without making drastic approximations and, in fact, have never before been solved in the literature *in any dimensions* (except for our own short report earlier⁶). In carrying out the full many-body dynamical calculations for the BSE we are forced to make some approximations. Our most sophisticated approximation uses the fully frequency-dependent dynamically screened electron-hole Coulomb interaction in the single-plasmon-pole approximation, which has been shown to be an excellent approximation²³ to the full RPA [see Fig. 2(c)] for the 1D QWR system. For the self-energy correction we use the single-loop GW diagram shown in Fig. 2(b) with the screened interaction given by the PPA. Ward identities then fix the vertex correction, entering Fig. 2(a), to be the appropriate ladder integral equation.

For convenience, we use the finite-temperature imaginary-time Matsubara frequency Green's function formalism in our analysis. The bare electron-hole two-particle Green's function without any e - h interaction is

$$G^0(k, k', z, \Omega) = G_e(k, \Omega - z) G_h(-k, z) \delta_{k, k'}, \quad (14)$$

and it corresponds to the two separate Green's function lines of electron and hole in Fig. 2(a). For each particle line, we have

$$G_i(k, z) = \frac{1}{z - \varepsilon_{i,k} - \Sigma_i(k, z) + \mu_i} \quad (i = e, h), \quad (15)$$

where $\varepsilon_{e,k} \equiv k^2/2m_e + E_g^0$ and $\varepsilon_{h,k} \equiv k^2/2m_h$ are the bare (noninteracting) band energies for electrons in the conduction band and for holes in the valence band, respectively; μ_i is the chemical potential and $\Sigma_i(k,z)$ is the self-energy (for a complex frequency z), which we will calculate later within the GW approximation. In order to avoid the multipole (and any possible branch cut) structure in $G_i(k,z)$, we approximate $\Sigma_i(k,z)$ by the momentum-dependent band-gap renormalization $\Delta_i(k)$, which is related to the self-energy through the self-consistent Dyson's equation $\Delta_i(k) = \Sigma_i(k, \varepsilon_{i,k} + \Delta_i(k) - \mu_i)$; i.e., $\Delta_i(k)$ is the so-called quasiparticle on-shell self-energy. However, $\Delta_i(k)$ can be well approximated²⁴ by truncating this equation at the first non-trivial order, i.e., $\Delta_i(k) = \Sigma_i(k, \varepsilon_{i,k} - \mu_i)$, which should be reasonably valid in our calculations below. Therefore we have the following electron-hole single-pole Green's function:

$$G_i(k,z) \sim \frac{1}{z - \varepsilon_{i,k} - \Delta_i(k) + \mu_i}, \quad (16)$$

for later calculations in this paper. The details of calculating the self-energy $\Sigma_i(k,z)$ within the GW approximation are discussed in the Sec. IID below.

The Bethe-Salter equation in Fig. 2(a) could be read as (with $\beta = 1/k_B T$, where T is the temperature)

$$\begin{aligned} G(k,k',z,\Omega) &= G^0(k,k',z,\Omega) \\ &\times \left(1 + \frac{1}{\beta} \sum_{k'',z'} V_s(k-k'',z-z') G(k'',k',z',\Omega) \right). \end{aligned} \quad (17)$$

Putting Eqs. (14)–(16) into Eq. (17) we get

$$\begin{aligned} &[\Omega - \varepsilon_{e,k} - \varepsilon_{h,-k} - \Delta_e(k) - \Delta_h(-k) \\ &+ \mu_e + \mu_h] G(k,k',z,\Omega) \\ &= [G_e(k,\Omega-z) + G_h(-k,z)] \delta_{k,k'} \\ &\times \left(1 + \frac{1}{\beta} \sum_{k'',z'} V_s(k-k'',z-z') G(k'',k',z',\Omega) \right). \end{aligned} \quad (18)$$

This equation, however, is not of closed form and is difficult to evaluate since it is a rather complex multidimensional singular integral equation. We therefore have to use an additional simplifying approximation first introduced by Shindo,^{18,25,26} where the two-particle Green's function $G(k,k',z,\Omega)$ is replaced by a simple pair Green's function $G(k,k',\Omega)$ [whose retarded function yields via Eq. (9) directly the optical dielectric function]:

$$\begin{aligned} G(k,k',z,\Omega) &\simeq \frac{G_e(k,\Omega-z) + G_h(-k,z)}{-\frac{1}{\beta} \sum_z [G_e(k,\Omega-z) + G_h(-k,z)]} G(k,k',\Omega), \end{aligned} \quad (19)$$

where

$$G(k,k',\Omega) \equiv -\frac{1}{\beta} \sum_z G(k,k',z,\Omega) \quad (20)$$

and

$$\begin{aligned} &-\frac{1}{\beta} \sum_z [G_e(k,\Omega-z) + G_h(-k,z)] \\ &= 1 - n_e(\xi_{e,k}) - n_h(\xi_{h,-k}). \end{aligned} \quad (21)$$

Here $\xi_{i,k} \equiv \varepsilon_{i,k} + \Delta_i(k)$ and $n_i(\xi_{i,k})$ is the fermion momentum distribution function $(e^{\beta(\text{Re} \xi_{i,k} - \mu_i)} + 1)^{-1}$, which keeps the electron and hole density constant by adjusting the chemical potential μ_i to satisfy the correct density constraint $\int (dk/\pi) n_i(\xi_{i,k}) = n$. Note that the approximation defined by Eq. (19) follows from the exact BSE in a statically screened Coulomb interaction,²⁵ i.e., if the frequency dependence of the effective dynamically screened interaction is neglected. We expect the Shindo approximation to be a reasonable approximation in our dynamical calculation below, because the dynamical screening effect contributes mostly to the correlation energy, whose real part is dominated by the (static) Hartree-Fock exchange energy in the high-density region¹⁹ (while the imaginary part of the correlation energy plays an important role in our calculations below). We have not been able to find a tractable way of solving the dynamical BSE without making the Shindo approximation.

Using Eqs. (15) and (19)–(21) in Eq. (18), we then have the following effective Bethe-Salpeter equation for the pair Green's function $G(k,k',\omega)$ (after the analytical continuation $\Omega \rightarrow \omega + i\delta - \mu_e - \mu_h$):

$$\begin{aligned} G(k,k',\omega) &= G^0(k,k',\omega) \\ &\times \left(1 - \sum_{k''} V_{eff}(k'',k',\omega) G(k'',k',\omega) \delta_{ss''} \right), \end{aligned} \quad (22)$$

where G^0 and the dynamically screened effective electron-hole interaction V_{eff} are expressed as

$$G^0(k,k',\omega) = \frac{1 - n_e(\xi_{e,k}) - n_h(\xi_{h,-k})}{\omega + i\delta - \varepsilon_{e,k} - \varepsilon_{h,-k} - \Delta(k,\omega)} \delta_{k,k'} \quad (23)$$

and

$$\begin{aligned}
V_{eff}(k, k', \omega) &= \left(\frac{1}{\beta} \right)^2 \sum_{z, z'} \left[\frac{G_e(k, \Omega - z) + G_h(-k, z)}{1 - n_e(\xi_{e,k}) - n_h(\xi_{h,-k})} \right. \\
&\quad \times V_s(k - k', z - z') \\
&\quad \left. \times \frac{G_e(k', \Omega - z') + G_h(-k', z')}{1 - n_e(\xi_{e,k'}) - n_h(\xi_{h,-k'})} \right]_{\Omega = \omega - \mu_e - \mu_h + i\delta}. \quad (24)
\end{aligned}$$

The effective BGR $\Delta(k, \omega)$ is given by

$$\begin{aligned}
\Delta(k, \omega) &= \sum_{k'} \{ [1 - n_e(\xi_{e,k'+q}) - n_h(\xi_{h,-k'})] \\
&\quad \times V_{eff}(k, k', q, \omega) - V_c(k - k') \} \\
&= - \sum_{k'} [n_e(\xi_{e,k'+q}) + n_h(\xi_{h,-k'})] V_{eff}(k, k', \omega) \\
&\quad + \sum_{k'} [V_{eff}(k, k', q, \omega) - V_c(k - k')]. \quad (25)
\end{aligned}$$

In Eq. (25) the self-energy term $(n_e + n_h)V_{eff}$ and the vertex correction $V_{eff} - V_c$ are treated on an equal footing. $G^0(k, k', \omega)$ in Eq. (23) is the electron-hole pair Green's function with self-energy correction but without electron-hole attractive interaction, which is now replaced by the dynamically screened effective interaction $V_{eff}(k, k', \omega)$ in the BSE, Eq. (22). If we neglect dynamical effects in $V_s(k, z)$ (as in the static or the quasistatic approximation described below), then $V_{eff}(k, k', \omega) = V_s(k)$ according to Eqs. (24) and (21). In the following section, we will discuss the use of different screening models to evaluate $V_{eff}(k, k', \omega)$ [and BGR $\Delta_{e/h}(k)$ through the screened GW approximation] in calculating the absorption spectrum by solving the BSE.

Combining the Bethe-Salpeter equation (22) for $G(k, k', \omega)$ with Eq. (12), we have the following equation for $Q(k, \omega)$:

$$Q(k, \omega) = Q_0(k, \omega) \left(1 - \frac{1}{M(k)} \sum_{k'} V_{eff}(k, k', \omega) Q(k', \omega) \right), \quad (26)$$

for $Q_0(k, \omega) \equiv \sum_{k'} M(k') G^0(k, k', \omega)$. Once $Q(k, \omega)$ is obtained by solving the integral equation (26), which is also a BSE, it is straightforward to calculate the absorption and gain spectra from the dielectric function $\varepsilon(\omega)$ through Eq. (13).

D. Self-energy, BGR, and screening in QWR's

In order to solve Eqs. (22)–(26) for the Bethe-Salpeter equation, we have to use a screened interaction $V_s(k, z)$ in Eq. (24) to get V_{eff} and also to get the single-particle self-energy $\Sigma_i(k, z)$ in the Green's function of Eq. (16). In this section, we discuss and compare both the quasistatic approximation and the dynamical (PPA) approximation in the

screening calculation. For convenience, we first discuss the self-energy part and then the screening effect.

In the GW approximation, which is the leading-order self-energy in the screened interaction expansion, the self-energy is calculated in the single-loop diagram composed of a non-interacting particle line and a screened interaction line [Fig. 2(b)]. Using static screening in the interaction line [i.e., $V_s(k, z) = V_s(k, 0)$], we get a screened exchange self-energy term only, and all higher-order screening effects to the correlation energy are neglected. This approximation (named the static approximation) is therefore too simplistic to give correct results,⁶ although it has been extensively employed in excitonic calculations because of its simplicity. An improvement to the static approximation is the quasistatic approximation,¹⁸ which neglects the recoil energy during the scattering process so that no dynamical frequency inside the screened interaction potential shows up. This approximation produces an extra constant Coulomb-hole term [the second term of Eq. (27)] in the self-energy in addition to the screened exchange self-energy of the static approximation, so that the full expression for the BGR in this quasistatic approximation becomes

$$\Delta_i(k) = \sum_{k'} \left[-V_s(k - k') n_i(\varepsilon_{i,k}) + \frac{1}{2} [V_s(k') - V_c(k')] \right], \quad (27)$$

where $V_s(k) \equiv V_s(k, \omega = 0) = V_c(k) / \varepsilon(k, \omega = 0)$ is the statically screened Coulomb interaction, which could be analytically derived either from the RPA [using Eq. (29) below] (Ref. 15) or PPA [using Eq. (30) below].²³ In our paper, the former is named the quasistatic RPA and the latter named the quasistatic PPA. Note that $\Delta_i(k)$ in Eq. (27) is pure real, i.e., without any imaginary part of the self-energy or inelastic broadening effect, so that the quasiparticle assumption for the Landau-Fermi liquid is completely satisfied in this approximation with an infinite quasiparticle lifetime. It is well known, however, that the quasiparticle assumption breaks down in 1D (unlike in 2D or 3D) electronic systems, with a generic non-Fermi-liquid behavior.²⁷ For the purpose of comparison we still use this approximation to calculate the 1D optical properties in order to compare with the full dynamical calculation results and to study the quantitative validity of this widely used quasistatic approximation both in the higher-dimensional systems^{18,22} and in the 1D system^{7,10} in the literature. In Fig. 3(a) we show the conduction-band energy $\xi_{e,k}^0 - E_g^0 = \varepsilon_{e,k} + \Delta_e(k) - E_g^0$ in the quasistatic PPA for different electron densities. The band-gap renormalization is almost a wave-vector-independent rigid shift in the quasistatic approximation.

For the self-energy $\Sigma_i(k, \omega)$ calculated in the one-loop GW approximation with dynamically screened interaction, we have

$$\begin{aligned}
\Sigma_i(k, z) &= - \frac{1}{\beta} \sum_{k', z'} V_s(k - k', z - z') G_i(k', z') \\
&= - \frac{1}{\beta} \sum_{k', z'} \frac{V_c(k - k')}{\varepsilon(k - k', z - z')} G_i(k', z'), \quad (28)
\end{aligned}$$

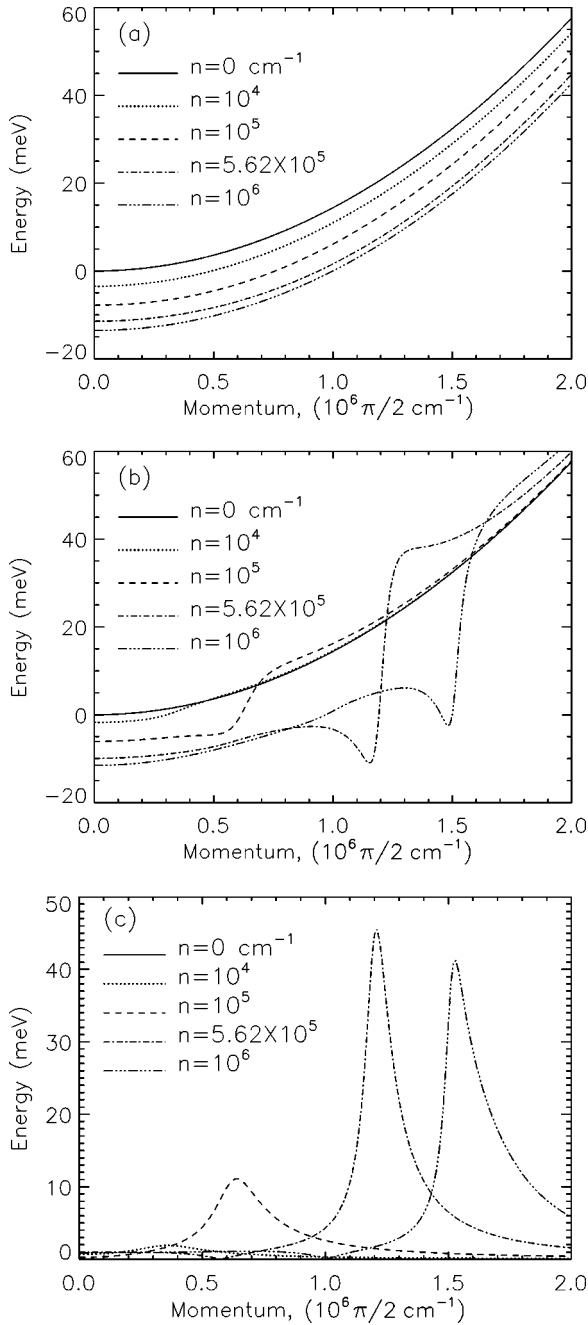


FIG. 3. (a) Conduction-band energy $\xi_{e,k} - E_g^0$ calculated in the GW approximation with screened interaction approximated by the quasistatic PPA. (b) and (c) are, respectively, the real and imaginary parts of the band energy calculated in the dynamically screened GW approximation (within PPA) for the same system as (a). The calculation is carried out in the symmetric T-shaped QWR system with $W_y = W_z = 7 \text{ nm}$ including finite-temperature ($T = 10 \text{ K}$) and finite (phenomenological) impurity scattering ($\gamma = 0.5 \text{ meV}$) effects.

where we can use either the RPA or PPA [which is an excellent approximation to the RPA (Ref. 23)] to calculate the dynamical dielectric function $\varepsilon(k, \omega)$. For the zero-temperature RPA, $\varepsilon(k, \omega)$ is obtained by including the non-interacting polarizabilities of electrons [$\Pi_e^0(k, \omega)$] and holes [$\Pi_h^0(k, \omega)$] (Ref. 15):

$$\begin{aligned} \varepsilon(k, \omega) &= 1 - V_c(k) \Pi_e^0(k, \omega) - V_c(k) \Pi_h^0(k, \omega) \\ &= 1 - V_c(k) \sum_{i=e,h} \frac{m_i}{\pi k} \ln \left[\frac{\omega^2 - [(k^2/2m_i) - kv_{F,i}]^2}{\omega^2 - [(k^2/2m_i) + kv_{F,i}]^2} \right], \end{aligned} \quad (29)$$

where $v_{F,e/h}$ is the (Fermi) velocity of electrons or holes at Fermi momentum in the conduction and valence bands. In this paper we will use the RPA only in calculating the quasistatic screening via Eq. (27) by setting $\omega = 0$ in Eq. (29), not in the full dynamical BSE [Eq. (26)], because the pole structure (and branch cut properties) of the screened interaction, $V_c(k)/\varepsilon(k, \omega)$, in the full dynamical RPA is too complicated to deal with in the frequency summation of Eq. (24) and in the integral equation (26). In the dynamical PPA, however, the dielectric function $\varepsilon(k, \omega)$ is defined by the following expression where screening is induced by a single (plasmon) pole satisfying the corresponding f -sum rule:²³

$$\frac{1}{\varepsilon(k, \omega)} = 1 + \frac{\omega_{pl}^2(k)}{(\omega + i\delta)^2 - \omega_k^2}, \quad (30)$$

where $\omega_{pl}(q) = \sqrt{nV_c(q)q^2/m}$ is the 1D plasmon oscillator strength and ω_q is the effective plasmon frequency given by a simple formula^{14,18,23}

$$\omega_q^2 = \omega_{pl}^2(q) + \frac{nq^2}{m\kappa} + \frac{q^4}{4m^2}, \quad (31)$$

where κ is the inverse screening length. It has been shown that the PPA is a very good approximation to the RPA in 1D systems, where plasmon excitations dominate the single-particle excitations.^{15,23} The great virtue of the single-pole PPA for our theory is that it makes our calculation of V_{eff} in Eq. (24) tractable because the integral equation in frequency becomes simple. In the PPA the self-energy of the electron ($i=e$) or hole ($i=h$) can be expressed as a sum of the usual exchange or Hartree-Fock energy $\Sigma_i^{ex}(k)$ and the correlation energy $\Sigma_i^{cor}(k, \omega)$:

$$\Sigma_i(k, \omega) = \Sigma_i^{ex}(k) + \Sigma_i^{cor}(k, \omega),$$

$$\Sigma_i^{ex}(k) = - \sum_{k'} V_c(k') n_i(\varepsilon_{i,k'}),$$

$$\begin{aligned} \Sigma_i^{cor}(k, \omega) &= \sum_{k'} \frac{V_c(k') \omega_{pl}^2(k')}{2\omega_{k'}} \left[\frac{n_B(\omega_{k'}) + n_i(\varepsilon_{i,k+k'})}{\omega + \omega_{k'} - \varepsilon_{i,k+k} - i\gamma} \right. \\ &\quad \left. + \frac{n_B(\omega_{k'}) + 1 - n_i(\varepsilon_{i,k+k'})}{\omega - \omega_{k'} - \varepsilon_{i,k+k} + i\gamma} \right], \end{aligned} \quad (32)$$

where $n_B(\omega_k)$ is the bosonic momentum distribution function ($e^{\beta\omega_k} - 1$)⁻¹ for the plasmons; γ is a small phenomenological damping term incorporating impurity scattering and all other possible broadening processes (see the discussion in Sec. III B). From Eq. (32) we see that the dynamical effect as well as the imaginary part of $\Sigma_i(k, \omega)$ arises entirely from the correlation energy [and is absent in the static (Hartree-Fock) or quasistatic theory]. This will play an important role

(which is crucial in 1D) in our following calculations. Figures 3(b) and 3(c) show the real and imaginary parts of the electron energy $\xi_{e,k} - E_g^0 = \varepsilon_{e,k} + \Sigma_e(k, \varepsilon_{e,k} - \mu_e) - E_g^0$, taking into account the dynamical PPA self-energy renormalization.

Defining the on-shell self-energy to be $\Delta_i(k) \equiv \Sigma_i(k, \varepsilon_{i,k} - \mu_e)$ where $i = e, h$, the imaginary part of $\Delta_e(k)$ is proportional to the electron inelastic-scattering rate¹⁵ arising from electron-electron interaction, which is very small when k is below some threshold momentum k_c . For $k > k_c$ a new collective-mode scattering channel opens up in which electrons lose energy by emitting plasmons. At zero temperature and for zero impurity scattering (clean system limit), it can be shown that the inelastic-scattering rate diverges as $(k - k_c)^{-1/2}$ when k approaches k_c from above in 1D.¹⁵ Note that this divergence in $\text{Im} \Delta_{e/h}(k)$ also exists in the RPA calculation,¹⁵ and is therefore a characteristic of the interacting 1D system in the dynamical GW approximation, causing a gap to open up at $k = k_c$ in the real part of the self-energy as shown in Fig. 3(b). The existence of this gap in the BGR [or the divergence in $\text{Im} \Delta_{e/h}(k)$] reflects the breakdown of the quasiparticle picture in the 1D electron system²⁷ within the perturbative GW approximation. An interacting 1D electron system is known to be better described by the Luttinger liquid (LL) model than the Fermi liquid model due to the strong plasmon scattering effect arising from the limited phase space in 1D. A Luttinger liquid, in contrast to a Fermi liquid, does not have any discontinuity in its momentum distribution function, and does not, therefore, have any true quasiparticles. The existence of a Luttinger liquid is a purely nonper-

turbative effect of interaction and happens in 1D even for an arbitrarily weak electron-electron interaction. We therefore cannot get a true Luttinger liquid within our perturbative GW approximation, but the opening of the gap in the real part of the self-energy (or equivalently the divergence in the imaginary part of the self-energy) is the perturbative signature of the breakdown of the Fermi liquid picture. At finite temperature and for finite impurity scattering, the single-particle properties calculated in the 1D Fermi liquid model via the dynamical GW approximation are similar to the results calculated in the Luttinger liquid theory. Therefore we believe that the strong inelastic scattering shown in Fig. 3(c) qualitatively reflects the LL character of 1D systems, and our self-energy calculation is qualitatively correct for our purpose of calculating excitonic optical properties. Our inclusion of the strong inelastic scattering by plasmons catches some essential aspects of the 1D phase-space restriction, which eventually leads to the nonperturbative formation of a 1D Luttinger liquid, which is beyond the scope of this work.

We evaluate the effective interaction V_{eff} in Eq. (24) by using the same PPA approximation and obtain

$$V_{eff}(k, k', \omega) = V_c(k - k') \times \left[1 + \frac{1}{N_{eh}(k)} \frac{1}{N_{eh}(k')} \chi_{eh}(k, k', \omega) \right], \quad (33)$$

where $N_{eh}(k) \equiv 1 - n_e(\xi_{e,k}) - n_h(\xi_{h,k})$ and χ_{eh} is given by the the following complicated formulas containing eight different terms associated with various dynamical processes in the 1D e - h system:

$$\begin{aligned} \chi_{eh}(k, k', \omega) = & \frac{\omega_{pl}^2(k - k')}{2\omega_{k-k'}} \left[\frac{-[1 + n_B(\omega_{k-k'})]n_e(\xi_{e,k}) + n_B(\omega_{k-k'})n_e(\xi_{e,k'}) + n_e(\xi_{e,k})n_e(\xi_{e,k'})}{\xi_{e,k} - \xi_{e,k'} - \omega_{k-k'}} \right. \\ & + \frac{-n_B(\omega_{k-k'})n_e(\xi_{e,k}) + [1 + n_B(\omega_{k-k'})]n_e(\xi_{e,k'}) - n_e(\xi_{e,k})n_e(\xi_{e,k'})}{\xi_{e,k} - \xi_{e,k'} + \omega_{k-k'}} \\ & + \frac{-[1 + n_B(\omega_{k-k'})]n_h(\xi_{h,-k}) + n_B(\omega_{k-k'})n_h(\xi_{h,-k'}) + n_h(\xi_{h,-k})n_h(\xi_{h,-k'})}{\xi_{h,-k} - \xi_{h,-k'} - \omega_{k-k'}} \\ & + \frac{-n_B(\omega_{k-k'})n_h(\xi_{h,-k}) + [1 + n_B(\omega_{k-k'})]n_h(\xi_{h,-k'}) - n_h(\xi_{h,-k})n_h(\xi_{h,-k'})}{\xi_{h,-k} - \xi_{h,-k'} + \omega_{k-k'}} \\ & + \frac{n_e(\xi_{e,k})n_h(\xi_{h,-k'}) + [1 + n_B(\omega_{k-k'})][1 - n_e(\xi_{e,k}) - n_h(\xi_{h,-k'})]}{\omega + i\gamma + \mu_e + \mu_h - \xi_{e,k} - \xi_{h,-k'} - \omega_{k-k'}} \\ & + \frac{-n_e(\xi_{e,k})n_h(\xi_{h,-k'}) + n_B(\omega_{k-k'})[1 - n_e(\xi_{e,k}) - n_h(\xi_{h,-k'})]}{\omega + i\gamma + \mu_e + \mu_h - \xi_{e,k} - \xi_{h,-k'} + \omega_{k-k'}} \\ & + \frac{n_e(\xi_{e,k'})n_h(\xi_{h,-k}) + [1 + n_B(\omega_{k-k'})][1 - n_e(\xi_{e,k'}) - n_h(\xi_{h,-k})]}{\omega + i\gamma + \mu_e + \mu_h - \xi_{e,k'} - \xi_{h,-k} - \omega_{k-k'}} \\ & \left. + \frac{-n_e(\xi_{e,k'})n_h(\xi_{h,-k}) + n_B(\omega_{k-k'})[1 - n_e(\xi_{e,k'}) - n_h(\xi_{h,-k})]}{\omega + i\gamma + \mu_e + \mu_h - \xi_{e,k'} - \xi_{h,-k} + \omega_{k-k'}} \right], \quad (34) \end{aligned}$$

where we use the same phenomenological damping parameter γ to broaden the resonant threshold energies in the denominators. The first two terms in the brackets of Eq. (34) describe the coupling of electron excitations with the plasmon, having the corresponding particle filling factors in the numerator and the resonance energy in the denominator. The third and the fourth terms describe the same plasmon coupling process for the holes. The first four terms are static and ω independent in our approximation. The last four terms are dynamical and depend explicitly on ω . These last four dynamical terms describe processes which couple both electron and hole systems with the plasmon modes, and are extremely important in the dynamics of the photoexcited system. Note that we take the real part of χ_{eh} only in our numerical calculation because the Hermiticity of V_{eff} is required for the effective Hamiltonian shown below in Eq. (36).

E. Effective Hamiltonian and variational method

Before solving the full dynamical Bethe-Salpeter equation, it is instructive to study the excitonic and the EHP effects *separately* by treating the influence of the EHP on the excitonic states as a perturbation.^{18,26} Using an effective Hamiltonian derived from the Bethe-Salpeter equation, we can variationally obtain the exciton ground-state energy by minimizing the energy expectation value through a $1s$ exciton trial wave function. The effective Hamiltonian treats the EHP as a perturbative effect and is written as $H_{pp'}(\omega_n) = H_{pp'}^0 + H'_{pp'}(\omega_n)$, where

$$H_{pp'}^0 = \left(E_g^0 + \frac{p^2}{2m} \right) \delta_{pp'} - V_c(p-p') \quad (35)$$

is the Hamiltonian for the single electron-hole pair with an unscreened Coulomb interaction (similar to a 1D hydrogen atom) and the perturbation H' is

$$H'_{pp'}(\omega_n) = \Delta(p, \omega_n) \delta_{pp'} + V_c(p-p') - [1 - f_e(\xi_{e,p}) - f_h(\xi_{h,-p})] V_{eff}(p, p', \omega_n), \quad (36)$$

for the n th eigenstate of energy ω_n . Here we can explicitly see the physical meaning of $\Delta(p, \omega)$ and $V_{eff}(p, p', \omega)$ analytically derived in Eqs. (24) and (25). We expect that the wave function of the exciton satisfies the corresponding Schrödinger's equation in the low-density limit, where the screening effect is negligible. Thus this exciton effective Hamiltonian approach may be a reasonable approximation to calculate exciton energies and wave functions.

For the exciton trial wave function $\phi_n(p)$ in momentum space, we use the two-parameter variational wave function first introduced by Nojima^{7,8} to express the 1D exciton ground state as

$$\phi_0(p) = \sqrt{\frac{2\sigma\lambda}{K_1(2\sigma)}} \frac{K_1(\sigma\sqrt{\lambda^2 p^2 + 1})}{\sqrt{\lambda^2 p^2 + 1}}, \quad (37)$$

where λ and σ are two independent (positive) variational parameters in our calculation. $K_1(x)$ is the first-order modi-

fied Bessel function of the second kind. This variational bound-state wave function has the following form in real space:

$$\phi_0(x) = \frac{\exp[-\sqrt{(x/\lambda)^2 + \sigma^2}]}{\sqrt{2\sigma\lambda} K_1(2\sigma)}, \quad (38)$$

where one can see that the variational parameter λ represents the exciton radius and σ smoothes or broadens the center-of-mass wave function at $x=0$. We do not study the first excited-state wave function $\phi_1(p)$ in this paper because it is not particularly relevant to the Mott transition process we are interested in, although the variational technique can be adapted to study excited excitonic states.⁸

III. RESULTS

We first show the variational results because conceptually this is the simplest approach since it is based on an effective single-particle Hamiltonian. We obtain the BGR and the exciton binding energy by the variational method in both the quasistatic approximation and the dynamically screened GW approximations (within PPA) for various photoexcited carrier (e - h) densities. The crossover between the exciton energy and the BGR gives us an estimated Mott transition critical density n_c , where the exciton bound state ceases to exist and an insulator-to-metal transition occurs. The idea here is that at n_c the exciton merges with the e - h continuum and is no longer a stable bound state. Finally we carry out the full Bethe-Salpeter integral equation solution by a matrix inversion method and obtain the absorption spectra and refractive index in a large range of e - h density (from 10^2 to 10^6 cm^{-1}) to compare with the variational effective Hamiltonian results. Details are described below.

A. Effective Hamiltonian result

In Fig. 4(a), we show the calculated density dependence of the exciton ground-state energy variationally obtained from the effective Hamiltonian method and the BGR [$\Delta_e(0) + \Delta_h(0)$] calculated in both the quasistatic approximation and the dynamically screened GW approximation as described in Sec. II D. Both the RPA and PPA are used in the quasistatic calculation [Eq. (27)] for comparison whereas the full dynamical calculations are done only in the PPA. The intersection between the exciton energy (dashed lines) and the BGR (solid lines) indicates the Mott transition, where the exciton merges with the band continuum and the system has a phase transition from an insulating exciton gas to a conducting EHP. Note that the variational method introduced in Sec. II E loses its accuracy near the Mott density (and becomes essentially meaningless for $n > n_c$), because the variational energy expectation value $E(\lambda, \sigma) \equiv \langle \phi_0(\lambda, \sigma) | H^0 + H'(E(\lambda, \sigma)) | \phi_0(\lambda, \sigma) \rangle$ has a very flat minimum region in the λ - σ space around $n \approx n_c$; i.e., the exciton wave function is highly broadened, so that its minimum energy is hard to determine in such a perturbation-based variational method. In Fig. 4(b) we show the variationally calculated trial exciton $1s$ (ground-state) wave function $\phi_0(x)$ for different exciton

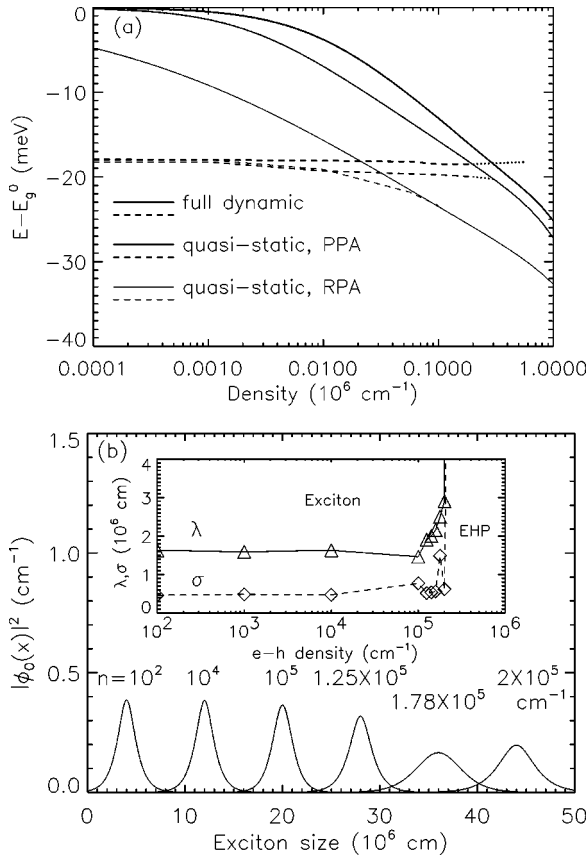


FIG. 4. (a) Separately variationally calculated exciton energy (dashed lines) and BGR of the EHP (solid lines) as a function of photoexcitation density, in three different approximations as indicated in the plot by different linewidths. Note that when the density is larger than $2 \times 10^5 \text{ cm}^{-1}$, the variational method (introduced in Sec. II E) fails to give a good exciton energy (see the text) and the dotted lines are the exciton peak positions of the corresponding absorption spectra by solving the BSE (Fig. 5). (b) The $1s$ exciton ground-state wave function obtained in the variational method through effective Hamiltonian [Eqs. (35) and (36)] in the dynamical (PPA) screening calculation for various electron-hole densities. Inset: the variational parameters λ and σ for the $1s$ exciton ground-state trial wave function with respect to the photoexcitation density in logarithm scale. When the density is near the Mott density ($n_c \sim 3 \times 10^5 \text{ cm}^{-1}$), both λ and σ increase sharply and the wave function becomes totally broadened.

densities. The exciton density dependences of the variational parameters λ and σ are also shown in the inset of Fig. 4(b). The sharp divergences of λ and σ at $n_c \sim 2 \times 10^5 \text{ cm}^{-1}$ indicate the delocalization of the exciton ground-state wave function, a signal of an exciton-to-EHP Mott transition. In Fig. 4(a) we terminate the variationally calculated exciton line (dashed) at $n = 2 \times 10^5 \text{ cm}^{-1}$ and use the dotted line to represent the peak position of the absorption spectra obtained from solving the full dynamically screened BSE (discussed below) to continue the exciton line to higher densities up to $6 \times 10^5 \text{ cm}^{-1}$.

We can make the following comments about the results shown in Fig. 4(a): (i) For a density below 10^4 cm^{-1} the exciton energy has only a few-meV density-dependent red-

shift in the quasistatic RPA/PPA approximations and almost no shift (less than 0.5 meV) in the dynamical screening approximation. This shows the almost complete cancellation between the exchange-correlation-induced BGR (a density-dependent shift) and the blueshift of the exciton energy (due to screening) over a wide range of density. On the other hand, using the static screening (i.e., exchange energy only) approximation in the same calculation does not lead to this cancellation,⁶ showing that the experimentally observed constancy of the exciton energy as a function of the photoexcited $e-h$ density is a dynamical effect, which may not manifest itself in simpler approximations. (ii) For an $e-h$ density higher than 10^4 cm^{-1} , the exciton energy in the quasistatic RPA has a rather large redshift until it merges with the BGR line smoothly at $n_c \sim 6 \times 10^4 \text{ cm}^{-1}$, indicating a rather low-density Mott transition in this system. On the other hand, the exciton energies calculated in both the quasistatic PPA and the full dynamical PPA are almost constant up to $n = n_c \sim 3 \times 10^5 \text{ cm}^{-1}$, where the band continuum meets the exciton energy. (iii) In the full dynamical results obtained by solving the dynamical BSE directly, the excitonic absorption peak (dotted line) seems to survive even for densities higher than the “critical density,” n_c , at which the calculated exciton energy crosses the band continuum BGR line. This shows that there must be reasonably strong hybridization between the exciton and the EHP in the dynamical BSE [note that the dotted line in Fig. 4(a) is not from the variational calculation, but is obtained from the BSE solution], so that the effective BGR, including excitonic effects in the BSE, is actually less than the result we calculate from Eq. (32) by adding the electron and hole self-energies without incorporating exciton effects. This also demonstrates the limitation of the quasistatic approximation and confirms the necessity of the full dynamical BSE calculation in the high-density 1D $e-h$ system.

B. Dynamical Bethe-Salpeter equation result

In Fig. 5, we show our calculated absorption and gain spectra by solving the full Bethe-Salpeter (integral) equation in the quasistatic and the full dynamical screening approximations for $W_y = W_z = 7 \text{ nm}$ wire at a low temperature of $T = 10 \text{ K}$. The integral equation for the two-particle Green’s function, Eq. (26) [or equivalently Eq. (22)], is solved by the matrix inversion method with maximum momentum up to $k_{\text{max}} = (\pi/2) \times 10^8 \text{ cm}^{-1}$ ($= 100k_F$ for $n = 10^6 \text{ cm}^{-1}$). The poles of the dynamical screened interaction V_{eff} in Eqs. (33) and (34), together with the logarithmic singularity of the 1D Coulomb interaction in the long-wavelength limit, produce a multisingular kernel with multiple momentum-dependent singularities which have never been solved before in the literature (except for our earlier work,⁶) because the usual singularity-removal method is ineffective here.^{18,22} In our calculations presented in this paper, we use a rather large matrix (1500×1500 in a Gaussian quadrature for $|k| \leq k_{\text{max}}$) in the matrix inversion method in order to get good overall accuracy; i.e., the same calculations using even larger (2000×2000) matrix size (which is extremely time consuming and not shown here) do not show any significant differ-

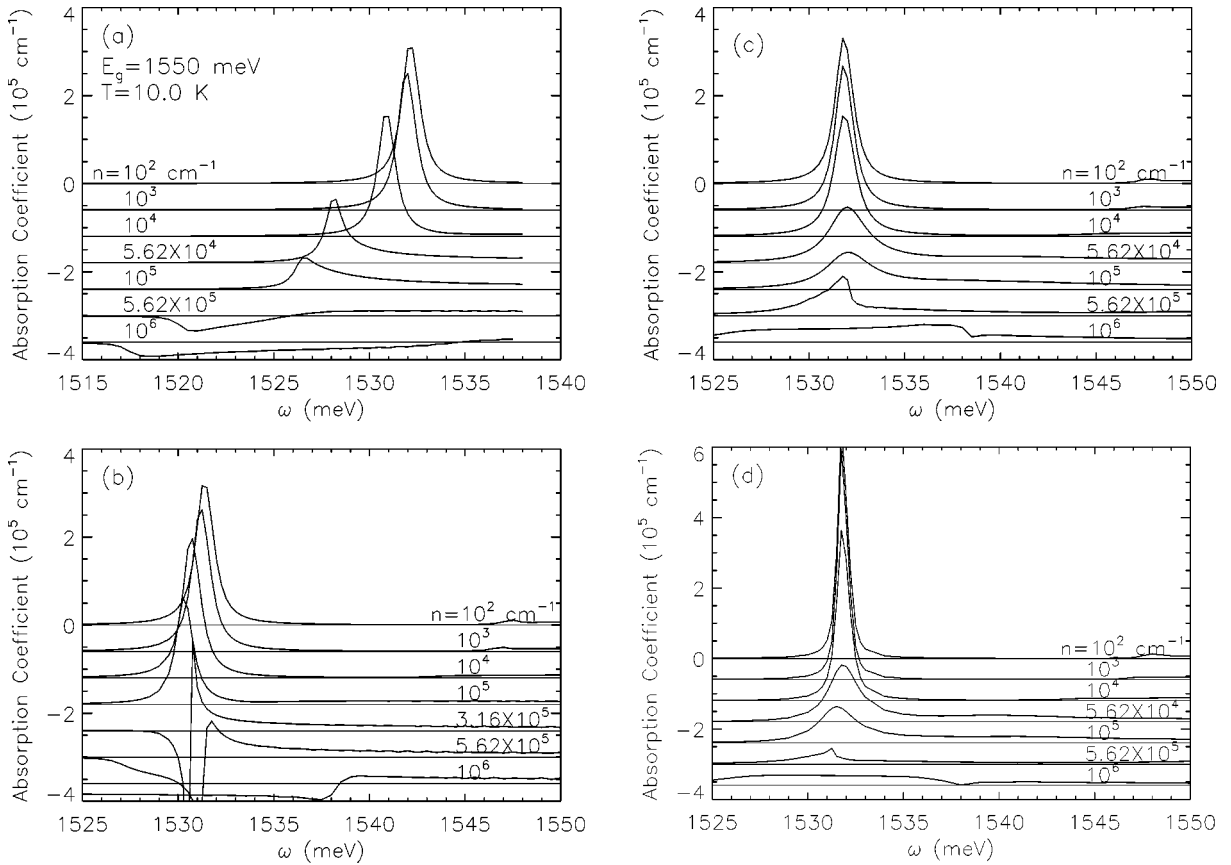


FIG. 5. Calculated absorption and gain spectra for various photoexcitation densities by solving the Bethe-Salpeter equation in three different approximations for screening: (a) the quasistatic RPA, (b) the quasistatic PPA, and (c) and (d) the full dynamical (PPA) calculation. The system parameters of (a)–(d) are the same as used in Fig. 3, except for the smaller γ ($=0.2$ meV) used in (d).

ence (within 10%) in the whole absorption (and refractive index) spectrum from the results we present in Figs. 5–7. The broadening γ used in our calculation is a phenomenological parameter which simulates in a simple manner the effects of all possible scattering and broadening processes not explicitly included in our theory. These are, for example, impurity and defect scattering, inhomogeneities in the system (e.g., fluctuations in the wire width), broadening associated with optical excitation process itself, and phonon scattering. We mention that inelastic plasmon scattering lifetime effects are explicitly included in our theory. Note that γ should be small compared with the bare excitonic binding energy (~ 10 – 20 meV in GaAs semiconductor QWR systems), and as long as γ is small, its precise value has no qualitative effect on our conclusions and results. We typically choose $\gamma=0.5$ meV in our calculations.

In Figs. 5(c) and 5(d) we show the absorption spectra in the dynamical PPA for two different values of impurity scattering γ (different by a factor of 2.5) to show that γ does not affect the qualitative behavior of the spectra, but does control the linewidths of the absorption peaks as one would expect. Some important features of the optical spectra (calculated by solving the full BSE) shown in Fig. 5 are the following: (i) there are generally two absorption peaks in the low-density ($n < 10^4$ cm $^{-1}$) spectra of all three approximations, one the exciton ground-state ($1s$) peak at about 1532 meV and the

other one the exciton first excited state ($2s$) at, for example, 1547.5 meV for $n = 10^2$ cm $^{-1}$ [this peak is off the plot region in Fig. 5(a)]. Note that this low-density spectrum is almost the same in all three different approximations, showing that the dynamical effect is not important in the low-density region. (ii) When the density increases but is still less than 10^4 cm $^{-1}$, the exciton peak does not shift much (< 2 meV) with increasing carrier density in all approximations, indicating the constancy of the exciton energy. (iii) At higher densities (10^4 cm $^{-1} < n < 10^5$ cm $^{-1}$), however, the quasistatic RPA result [Fig. 5(a)] shows some additional redshift in the excitonic peak, consistent with the result shown in Fig. 4(a) which is obtained from the variational method. On the other hand, the excitonic peak positions in the quasistatic PPA and in the full dynamical approximation are almost (density independent) constants in this region. A significant difference between the quasistatic PPA and the dynamical calculation results, however, is that the exciton peak of the quasistatic PPA results [Fig. 5(b)] has an almost constant oscillator strength, while the oscillator strength of the peak in the full dynamical calculation results [Fig. 5(c)] decays at high density to about one-third of its low-density value. (iv) For $n > 10^5$ cm $^{-1}$, both quasistatic RPA and quasistatic PPA results show negative absorption (gain) for the photon frequency below some critical value ω_c , while the full dynamical result is still positive (i.e., no gain) with a

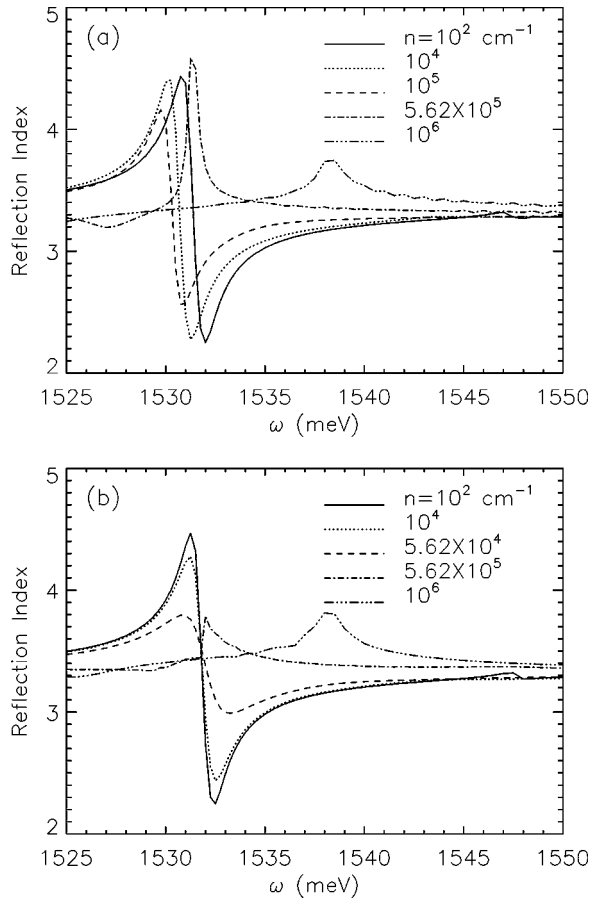


FIG. 6. Calculated refractive index for various photoexcitation densities in both (a) the quasistatic PPA and (b) the dynamical (PPA) approximation for interaction screening.

weaker broadened peak up to $n \approx 6 \times 10^5$ cm $^{-1}$ or higher. In other words, we do not explicitly find the expected exciton (insulator) to plasma (metal) Mott transition when both the self-energy and the screened interaction are included dynamically in the full BSE theory up to a rather high e - h density. We believe that this behavior arises from the strong plasmon scattering effects in 1D as discussed in Sec. IV of this paper. (Such strong inelastic scattering was not included in our earlier short report,⁶ leading to the appearance of a gain in the high-density spectra above the Mott density.) In Fig. 6, we show the refractive index $n(\omega)$ calculated by solving the Bethe-Salpeter equation in both the quasistatic PPA and the full dynamical approximation for different photoexcitation densities. The calculated refractive indices in these two approximations are similar in structure.

In Fig. 7, we show the calculated absorption-gain spectra obtained in both the quasistatic PPA [Fig. 7(a)] and the full dynamical calculations [Fig. 7(b)] for the same wire width $W_y = W_z = 7$ nm, but at a higher temperature ($T = 100$ K) for various densities. We find that the higher-temperature (100 K) low-density ($n < 10^4$ cm $^{-1}$) absorption spectrum is almost the same as the corresponding lower-temperature ($T = 10$ K) spectra in Figs. 5(b) and 5(c), while in the higher-density region ($n > 10^4$ cm $^{-1}$) the high-temperature exciton absorption peak of the full dynamical calculation has a

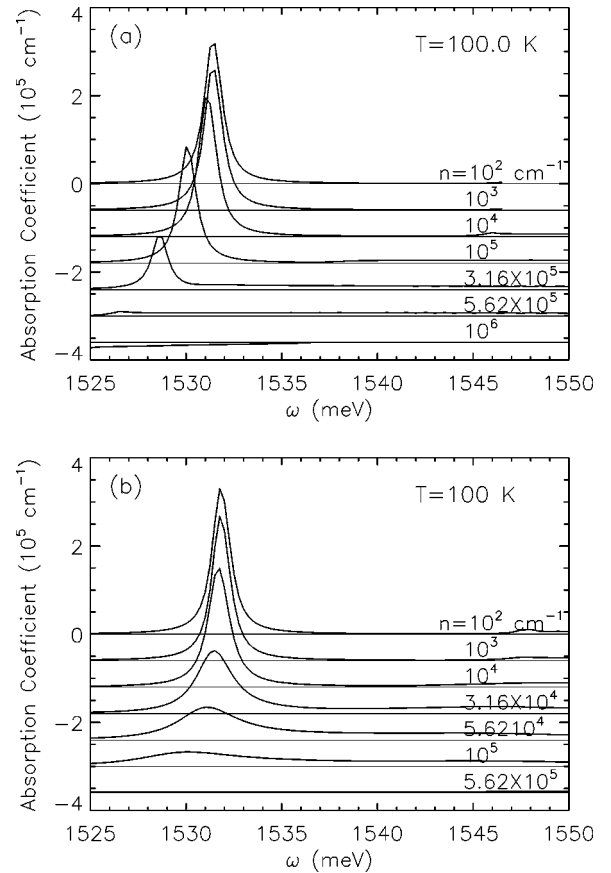


FIG. 7. Absorption and gain spectra obtained by solving the Bethe-Salpeter equation in (a) the quasistatic PPA and (b) the full dynamical (PPA) approximation for screening at high temperature ($T = 100$ K). Other system parameters are the same as used in Fig. 3.

smaller redshift in energy with a much larger broadening than the quasistatic PPA result. The quasistatic RPA result at such high temperature (not shown here) has an even larger redshift and broadening. We mention that the gain in the absorption spectra of the quasistatic calculation at the lower temperature [Fig. 5(b)] is flattened and almost disappears in the higher-temperature (100 K) calculation results.

IV. CONCLUSION

In this paper, we theoretically study, using a reasonably realistic Coulomb interaction, the excitonic optical properties of a 1D QWR system by solving the many-body Bethe-Salpeter equation using a number of approximations, the most sophisticated one being a treatment of both the self-energy and the vertex function in the dynamically screened GW approximation. Our calculation is applied to the experimentally studied T-shaped GaAs-Al $_x$ Ga $_{1-x}$ As 1D QWR systems for various densities and temperatures. We calculate the electron and hole self-energies in the one-loop GW approximation diagram using different screening approximations: the quasistatic RPA, the quasistatic PPA, and the dynamical (PPA) approximation. The quasistatic approximations give an almost rigid shift (the BGR effect) to the band energy [see

Fig. 3(a)], and there is no imaginary part of the self-energy; i.e., the quasiparticle lifetime is infinite. This approximation may work well in 2D and 3D systems but fails completely in 1D systems, because unlike in the higher-dimensional systems, the electrons in 1D system suffer a very strong inelastic-scattering effect by virtue of restricted phase space. Therefore the validity of the quasistatic approximation applied to 1D systems, which has been extensively used in many theoretical works,^{7,10,14,28,29} is doubtful. In the dynamical calculation we find that the electron and hole band-gap renormalization has a gap opening up in its real part and a consequent divergent singularity in its imaginary part at $k = k_c$ [Figs. 3(b) and 3(c)], where the quasiparticle energy is transferred to the plasmon excitations due to very strong inelastic scattering by 1D plasmons. Although this perturbative GW self-energy is “unphysical” due to the failure of the Fermi liquid model in the 1D system,²⁷ it still gives a rather good qualitative description of the single-particle and the collective-mode properties (compared to the correct Luttinger liquid model), particularly at finite temperatures and for finite impurity scattering.¹⁵ Our results in Figs. 3(b) and 3(c) reflect an important generic feature of 1D systems: the quasiparticle excitation has a very short lifetime (in fact, it does not exist) if the excitation momentum is higher than some value k_c . This 1D feature associated with the Luttinger liquid properties of 1D systems strongly affects the stability of 1D excitons and the bound quasielectron and quasihole pairs, as we can see from the calculated absorption and gain spectra (Fig. 5).

In Fig. 5 we find that the quasistatic approximation, which excludes inelastic scattering, gives rise to a negative absorption (gain) region in the highly photoexcited system. The existence of gain means that the exciton state is saturated (fully occupied), and therefore manifests a spontaneous emission, rather than absorption. On the other hand, the overall positive absorption (no gain) spectrum found in the dynamical calculation [Fig. 5(c)] up to the highest density is caused by the large imaginary part of the electron-hole on-shell self-energy, $\text{Im} \Delta_{e/h}(k)$ [see Fig. 3(c) and Eq. (32)], which is proportional to the inelastic-scattering rate and results from the energy scattering through plasmon channel. In other words, the excitons, composed of bound pairs of quasielectrons and quasiholes, are unstable due to strong inelastic scattering by 1D plasmon excitations in the high-density region. Consequently, in the dynamical calculation, the exciton absorption peak is suppressed in strength and broadened in width as the photoexcitation density increases, leading to stronger plasmon scattering. The absorption spectrum does not exhibit a negative (gain) region even in the high-density regime because the quasiparticle EHP band continuum is so strongly inelastically scattered by plasmons that it is not a proper eigenstate (i.e., it decays) and is never saturated. The disappearance of the exciton line and the non-negativity in the absorption spectra (at the same time) in our dynamical calculation suggest that there is *no* insulator (exciton) to the metal (EHP) Mott transition in 1D systems, since both excitons and quasiparticles are strongly inelastically scattered by plasmons, leading to neither of them being well-defined coherent states of the high-density 1D system.

This result is consistent with the well-known non-Fermi-liquid properties of 1D electronic systems, where the quasiparticle (and hence the exciton) picture fails. The quasistatic approximation, which ignores any plasmon effect and works well in 2D and 3D systems,²⁸ does not work in 1D systems because the 1D excitation spectrum is completely dominated by plasmons.

Another clue in support of the importance of plasmons in such a high-density 1D e - h system comes from the temperature dependence of the absorption spectra shown in Fig. 7. Our results show that the high-temperature ($T=100$ K) absorption peak in the dynamical calculation [Fig. 7(b)] is suppressed and broadened so greatly that there is almost no spectral structure observed for $n \geq 10^5 \text{ cm}^{-1}$, while the high-temperature quasistatic PPA result [Fig. 7(a)] still has a rather strong peak at the same density. This is because the plasmon excitation occupancy, whose energy distribution function $n_B(\omega_k)$ follows the Bose-Einstein statistics, depends strongly on temperature, leading to a qualitative difference between the $T=10$ K and $T=100$ K results in the dynamical calculation, while such plasmon dynamics is not included in the quasistatic calculation. This characteristic strong temperature dependence is also consistent with very recent experimental results.³

Based on our results and the discussion above, we propose that a crossover from a low-density (essentially noninteracting) Fermi liquid to a high-density interacting non-Fermi liquid is occurring in the optical spectra of the 1D e - h system as the photoexcitation density increases [see Fig. 5(c)]. In the low-density limit, say, $n \leq 10^2 \text{ cm}^{-1}$, we have a dilute and noninteracting exciton system, whose absorption spectrum is independent of the many-body screening approximations we use — plasmons are just not that important in this regime. This shows that excitons in this situation are isolated quasielectron and quasihole pairs, reflecting the validity of the quasiparticle picture in the effective noninteracting Fermi liquid model in the low density limit. In the higher-density region, however, the plasmon effect on the quasiparticle self-energy becomes important, because the band curvature at $k=k_F$ is less for higher k_F (i.e., higher density) and the relative importance of collective-mode excitations (plasmons) is then strongly enhanced as in the Luttinger liquid model. Therefore the oscillator strength of the exciton absorption peak is then reduced and broadened in our dynamical calculation [Fig. 5(c)]. When the density is roughly the nominal “Mott transition” critical density n_c , where the band continuum energy equals the exciton energy [see Fig. 4(a)], the plasmon excitation becomes so dominant that both exciton and band continuum (EHP) states become unstable, showing a crossover to effectively non-Fermi-liquid properties. We therefore do not expect to see the real Mott transition from an excitonic insulator to an EHP metal in 1D highly photoexcited systems, in contrast to the results of previous theories. For an electron-hole plasma without any backward scattering in the usual Luttinger liquid model (no band curvature at all, which is unrealistic in our case), we can prove that gain in the optical spectra does exist below the Fermi energy at all densities with a complicated power-law singularity at the Fermi surface. Including the electron-

hole attractive backward interaction (assuming a short-ranged interaction as in the so-called g -ology formalism), the electron-hole system most likely undergoes a charge density wave ground state transition with a mass gap in the elementary plasmon excitation.³⁰ While this scenario is consistent with our results, further work for the excitonic effect at energy *far below* the Fermi energy is still needed, because the regular Luttinger liquid model cannot include band curvature in an appropriate way in order to study the Mott transition at an energy level around the band edge.

In reference to the experimental data, we note that our results from solving the dynamically screened Bethe-Salpeter equation are in excellent qualitative and quantitative agreement with recent experimental findings.^{1,2} In particular, the effective constancy of the exciton peak as a function of the photoexcited carrier density and the possibility of excitonic absorption well into the high-density regime (even for $n > 6 \times 10^5 \text{ cm}^{-1}$) turn out to be characteristic features of the full dynamical theory (but *not* of the static and the quasistatic approximations). A full dynamical self-consistent theory as developed in this paper is thus needed for an understanding of the recent experimental results. Moreover, we find that in our theory, the plasmon effect is crucial in the high-density regime, leading to the nonexistence of any observable Mott transition in our calculation. This is consistent with recent experimental results,^{1,2} which do not observe an actual Mott transition in the semiconductor QWR system even in the high-photoexcitation-density ($\sim 3 \times 10^6 \text{ cm}^{-1}$) regime. We emphasize that only our dynamical theory, and not the static or quasistatic approximation, is in agreement with the experimental results. We point out that the physical reason for the failure of static screening theory in the exciton calculation is that static screening strongly overestimates the screening strength by not allowing dynamical antiscreening effects. The constancy of the exciton energy in this problem arises from an approximate cancelation between the self-energy correction (the band-gap renormalization) and the vertex correction in the problem.

Before concluding we emphasize the various simplifying approximations made in our theory: (i) we consider an effec-

tive 1D exciton problem by appropriately integrating over the transverse dimensions of the quantum wire — a more complete theory should take into account the full 3D nature of the quantum wire structure; (ii) we treat dynamical screening in the plasmon-pole approximation for the purpose of simplification; (iii) we treat many-body effects in the single loop GW approximation along with the corresponding ladder vertex correction.

In summary, our main accomplishments reported in this paper are the following: (i) the *first* fully dynamical theory of a photoexcited electron-hole system in semiconductors which treats self-energy, vertex corrections, and dynamical screening in a self-consistent scheme within a realistic Coulomb interaction-based Bethe-Salpeter theory; (ii) a reasonable qualitative and quantitative agreement with the recent experimental observations of a constant (photoexcitation density-independent) excitonic absorption peak in energy, which in our dynamical theory arises from an approximate cancellation between the self-energy and the vertex corrections in the Bethe-Salpeter equation; (iii) inclusion of the plasmon effect in the quasiparticle self-energy calculation in our dynamical theory, leading to our theoretical proposal that *no* Mott transition should be observed in 1D electron-hole systems (at least in optical experiments) even at very high photoexcitation density—i.e., there should be no optical gain region; (iv) instead, we suggest an experimentally observable crossover from a low-density noninteracting Fermi liquid behavior (quasiparticle-exciton favored) to a high-density interacting non-Fermi-liquid behavior (no stable quasiparticles and excitons). A more precise and nonperturbative theoretical model for the high-density 1D electron-hole system is needed for future study — such a study should somehow incorporate both band curvature and Luttinger liquid behavior in analyzing the optical properties, although we believe that the qualitative features of such a theory are already contained in our work.

ACKNOWLEDGMENTS

This work has been supported by the U.S. ONR and the U.S. ARO.

¹R. Ambigapathy, I. Bar-Joseph, D. Y. Oberli, S. Haacke, M. J. Brasil, F. Reinhardt, E. Kapon, and B. Deveaud, Phys. Rev. Lett. **78**, 3579 (1997).

²W. Wegscheider, L. N. Pfeiffer, M. M. Dignam, A. Pinczuk, K. W. West, S. L. McCall, and R. Hull, Phys. Rev. Lett. **71**, 4071 (1993).

³J. Rubioi, L. N. Pfeiffer, A. Pinczuk, S. He, H. U. Baranger, K. W. West, and B. S. Dennis (unpublished).

⁴R. Rinaldi, G. Coli', A. Passaseo, and R. Cingolani, Phys. Rev. B **59**, 2230 (1999).

⁵S. Glutsch, F. Bechstedt, W. Wegscheider, and G. Schedelbeck, Phys. Rev. B **56**, 4108 (1997).

⁶S. Das Sarma and D. W. Wang, Phys. Rev. Lett. **84**, 2010 (2000). Note that there is a mistake in the reported wire size given in this paper: it should be $W_y = 7 \text{ nm}$ and $W_z = 14 \text{ nm}$, rather than

7 nm in both $y-z$ directions.

⁷S. Nojima, Phys. Rev. B **51**, 11 124 (1995).

⁸S. Nojima, Phys. Rev. B **50**, 2306 (1994).

⁹F. Tassone and C. Piermarocchi, Phys. Rev. Lett. **82**, 843 (1999).

¹⁰F. Rossi and E. Molinari, Phys. Rev. Lett. **76**, 3642 (1996).

¹¹T. Ogawa and T. Takagahara, Phys. Rev. B **44**, 8138 (1991).

¹²D. Brinkmann and G. Fishman, Phys. Rev. B **56**, 15 211 (1997); S. N. Walck, T. L. Reinecke, and P. A. Knipp, *ibid.* **56**, 9235 (1997); M. Grundmann and D. Bimberg, *ibid.* **55**, 4054 (1997).

¹³M. H. Szymanska, P. B. Littlewood, and R. J. Needs, cond-mat/0011266 (unpublished).

¹⁴S. Benner and H. Haug, Europhys. Lett. **16**, 579 (1991); B. Tantar, J. Phys.: Condens. Matter **8**, 5997 (1996); C. Gréus, A. Forchel, R. Spiegel, F. Faller, S. Benner, and H. Haug, Europhys. Lett. **34**, 213 (1996).

- ¹⁵B. Yu-Kuang Hu and S. Das Sarma, Phys. Rev. B **48**, 5469 (1993).
- ¹⁶E. H. Hwang and S. Das Sarma, Phys. Rev. B **58**, R1738 (1998).
- ¹⁷M. Stopa, cond-mat/9908349 (1999).
- ¹⁸H. Haug and S. Schmitt-Rink, Prog. Quantum Electron. **9**, 3 (1984).
- ¹⁹G. D. Manhan, *Many Particle Physics*, 2nd ed. (Plenum, New York, 1990); D. Pines and P. Nozières, *The Theory of Quantum Liquids* (Addison-Wesley, Reading, MA, 1989).
- ²⁰S. Das Sarma and W. Y. Lai, Phys. Rev. B **32**, 1401 (1985).
- ²¹W. Y. Lai and S. Das Sarma, Phys. Rev. B **33**, 8874 (1986).
- ²²H. Haug and S. Schmitt-Rink, J. Opt. Soc. Am. B **2**, 1135 (1985).
- ²³S. Das Sarma, E. H. Hwang, and Lian Zheng, Phys. Rev. B **54**, 8057 (1996).
- ²⁴T. M. Rice, Ann. Phys. (N.Y.) **31**, 100 (1965).
- ²⁵K. Shindo, J. Phys. Soc. Jpn. **29**, 287 (1970).
- ²⁶R. Zimmermann, K. Kilimann, W. D. Kraeft, D. Kremp, and G. Röpke, Phys. Status Solidi B **90**, 175 (1978).
- ²⁷For a review, see, for example, J. Voit, J. Phys.: Condens. Matter **5**, 8305 (1993).
- ²⁸See Ref. 22 and H. Schweizer, A. Forchel, A. Hangleiter, S. Schmitt-Rink, J. P. Lowenau, and H. Haug, Phys. Rev. Lett. **51**, 698 (1983).
- ²⁹L. Rota, F. Rossi, P. Lugli, and E. Molinari, Phys. Rev. B **52**, 5183 (1995).
- ³⁰T. Ogawa, Phys. Status Solidi B **188**, 83 (1995).